

Electron density study of the one-dimensional organic metal bis(thiodimethylene)-tetrathiafulvalene tetracyanoquinodimethane

E. Espinosa

Laboratoire de Cristallographie et Modélisation de Matériaux Minéraux et Biologiques, LCM³B, URA CNRS n°809, Faculté des Sciences, Université Henri Poincaré, Nancy 1, Boîte Postale 239, 54506 Vandoeuvre-lès-Nancy Cédex, France and Institut de Ciència de Materials de Barcelona, CSIC, Campus de la UAB, 08193 Bellaterra Barcelona, Spain

E. Molins

Institut de Ciència de Materials de Barcelona, CSIC, Campus de la UAB, 08193 Bellaterra Barcelona, Spain

C. Lecomte*

Laboratoire de Cristallographie et Modélisation de Matériaux Minéraux et Biologiques, LCM³B, URA CNRS n°809, Faculté des Sciences, Université Henri Poincaré, Nancy 1, Boîte Postale 239, 54506 Vandoeuvre-lès-Nancy Cédex, France (Received 17 December 1996)

The crystal structure, thermal vibrations, and electron density of the charge-transfer complex bis(thiodimethylene)-tetrathiafulvalene tetracyanoquinodimethane (BTDMTTF-TCNQ, formally $C_{10}H_8S_6^+ \cdot C_{12}H_4N_4^-$) have been analyzed using 130 K single-crystal x-ray-diffraction data up to a resolution of $(\sin \theta/\lambda)_{\max} = 1.35 \text{ \AA}^{-1}$. A multipolar pseudoatom density model was fitted against the 5145 observed data with $I > 3\sigma(I)$, $[R(F) = 0.023, R_w(F) = 0.022, \text{GoF} = 0.91]$ optimizing the set of $(n_1; \alpha)$ parameters of the Slater-type sulfur radial function. This electron-density study allows us to understand that the charge transfer between ions ($\approx 0.7 e$) involves only the external sulfur atom in the cation and that the charge-density-wave behavior appearing in this complex is in relation to the external sulfur hybridization. Furthermore, the topological characterization of the electron density shows the isolated character of the external sulfur atom in relation to the rest of the cation, and explains that charge transfer occurs via the interaction between the external sulfur atoms and the triple bonds $C \equiv N$ of the anion, concentrating the transferred charge mainly on nitrogens. The electrostatic potential calculated in the region of the charge transfer cation-anion is topologically similar to most hydrogen bonds, showing a typical saddle point between the donor and the acceptor atoms. [S0163-1829(97)09428-9]

I. INTRODUCTION

Since the pioneering work of Coppens *et al.* in 1979,¹ no other charge-density studies involving organic metals of the tetrathiafulvalene tetracyanoquinodimethane (TTF-TCNQ) family have been carried out. The main problems in studying these materials are due to the mechanical instability of the crystals under cooling and to their metallic behavior, leading to a noticeable handicap for the usual charge-density models,²⁻⁵ which are designed to fit localized charges around atoms. Furthermore, the presence of charge-density waves (CDW) modulates the structure, averaging the atomic positions along the modulation.

The one-dimensional (1D) organic conductor BTDMTTF-TCNQ ($C_{10}H_8S_6^+ \cdot C_{12}H_4N_4^-$) is a charge-transfer complex, for which crystalline electric and magnetic properties, band-structure calculations, as well as the temperature dependence of resistivity were presented in a previous paper.⁶ The prominent feature of BTDMTTF-TCNQ is that it behaves as an almost pure 1D metal, showing metallic character down to 26 K. In a previous paper, we also reported the room-temperature crystal structure [$R(F) = 0.033, N_{\text{obs}} = 1174$]. The room-temperature crystal packing was compared to other donor-TCNQ complexes, specially in relation to the replacement of the external groups in the donor molecule by sulfur atoms. Later, x-ray diffuse scattering, conventional

x-ray crystal structure, and electronic properties at room temperature (RT) and at $T = 130 \text{ K}$ [$R(F) = 0.033, N_{\text{obs}} = 5646$] were also reported with special emphasis on charge-transfer and charge-density-wave (CDW) phenomena.⁷ Figure 1 shows the ORTEP (Oak Ridge Thermal Ellipsoids Plot Program) view⁸ of the complex and the stacking along the *c* axis.

The present paper is devoted to the characterization of the topology of the electron density and the electrostatic properties in BTDMTTF-TCNQ, in order to understand its electronic properties. The $T = 130 \text{ K}$ high-resolution x-ray-diffraction data⁷ are used in this electron density study. This study initializes an approach in this kind of material, for which some physical properties are not yet well understood.

II. EXPERIMENTAL DETAILS

A. Crystal growth

Bis(thiodimethylene)-tetrathiafulvalene (BTDMTTF) was synthesized as previously reported^{9,10} and tetracyanoquinodimethane (TCNQ) was purchased from the Aldrich Co. and recrystallized before use. The BTDMTTF-TCNQ (1:1) complex was formed in a quantitative yield as a black microcrystalline powder when warm 1,1,2-trichloroethane solutions of donor and acceptor were mixed. Shiny black plate-



like crystals of BTDMTTF-TCNQ were obtained by slow diffusion (one month) of solutions of the neutral donor in carbon disulfide and the neutral acceptor in acetonitrile.

A high-quality single-crystal specimen of $0.06 \times 0.36 \times 0.38$ mm, previously selected for the room-temperature experiment, was used for the x-ray-diffraction experiment at $T = 130 \pm 3$ K. The x-ray source was graphite monochromatized Mo $K\alpha$ radiation from a sealed tube. Measurements were made on an Enraf Nonius CAD4 diffractometer, equipped with a nitrogen jet stream low-temperature system (Soterem N-jet) installed in a dry box to prevent ice formation on the crystal; the gas stream temperature was monitored to 110 ± 3 K at the nozzle, corresponding to a temperature of the crystal of 130 K as calibrated by using the paraferroelectric KDP transition (122 K).¹¹

of 25 reflections with $21 < 2\theta < 60^\circ$. Intensity data were recorded as ω - 2θ scan profiles to a resolution $(\sin \theta/\lambda)_{\max} = 1.35 \text{ \AA}^{-1}$ for a total of 21 505 reflections in the following way: for $\sin \theta/\lambda \leq 1.12 \text{ \AA}^{-1}$ all the reflections in one hemisphere were collected (14 121 reflections); after a conventional refinement against these data, higher-order intensities were calculated to $\sin \theta/\lambda = 1.35 \text{ \AA}^{-1}$ and only reflections with an estimated $I > 5\sigma(I)$ were collected in the hemisphere. All these reflections were collected at $\psi = 0^\circ$. During the data collection three standard reflections (5, -1 , 2), (13, 1, 1), (-8 , -4 , 3) were measured at 2 h intervals. The total scan width ($\Delta\omega$) was $1.1 + 0.34 \text{ tg } \theta$ with a fixed horizontal and vertical detector aperture of $4 \times 6 \text{ mm}^2$. A scan speed $v = d\omega/dt$ depending on the signal-to-noise ratio ($0.82 < v < 4.11^\circ \text{ min}^{-1}$) was used for all data collection. The total exposure time was 456 h and the total experiment time was 31 days for a total of 21 505 collected reflections (only two nonobserved reflections up to $\sin \theta/\lambda \leq 1.0 \text{ \AA}^{-1}$.) No diffractometer or temperature problem occurred during the experiment. Crystal data and some experimental details are given in supplementary material.⁴⁵

C. Data processing

Data reduction and error analysis were done using DREAR programs.^{12,13} Reflection integration limits were taken from a Lorentzian model of the peak width variations. Absorption effects were corrected with a Gaussian integration method¹⁴ ($\mu_{\text{calc}} = 0.69 \text{ mm}^{-1}$, transmission range: $0.82 < T < 0.97$). A polynomial fit to the slight decay of the standard reflections intensities (about $\sim 2\%$), over the 456 h x-ray exposure time, was applied to scale the data and derive the instrumental instability coefficient ($\langle p \rangle = 1.1\%$) used in the calculation of $\sigma^2(|F|^2) = \sigma_c^2(|F|^2) + (\langle p \rangle |F|^2)^2$. The 21 505 data with $\sin \theta/\lambda \leq 1.35 \text{ \AA}^{-1}$ were averaged with the $2/m$ symmetry to give 6885 unique data ($I > 0$) of which 5145 has $I > 3\sigma(I)$. The internal agreement was $R_{\text{int}}(F^2) = 0.017$ and 0.019 , for all data and for data up to $\sin \theta/\lambda < 0.7 \text{ \AA}^{-1}$, respectively, [$R_{\text{int}}(F^2) = 0.028$ for $\sin \theta/\lambda < 0.7 \text{ \AA}^{-1}$ before absorption correction].

III. MULTIPOLAR REFINEMENT AND CHOICE OF SULFUR RADIAL FUNCTION

A. High-order refinement

High-order (HO) refinement strategy is commonly applied in electron density studies to obtain the best estimation of atomic positional and thermal parameters of nonhydrogen atoms, because high-order reflections are mainly core electrons sensitive. HO refinement was performed against 1760 reflections with $1.0 < \sin \theta/\lambda < 1.35 \text{ \AA}^{-1}$ and $I > 3\sigma(I)$. All positional and anisotropic thermal parameters of non-H atoms were refined, except the y coordinates, and the U^{12} and U^{23} thermal parameters of S5, C1, C7, and C8 atoms (set to zero), which are placed at the crystallographic mirror. Convergence was achieved at $R(F) = 0.044$, $R_w(F) = 0.045$, and $S = 0.85$ [for definitions of $R(F)$, $R_w(F)$, and S , see Table I]. The residual electron density in the planes of both donor and acceptor molecules ranges $-0.10 < \Delta\rho_{\text{res}} < 0.10 e \text{ \AA}^{-3}$. An anharmonic model (third-order Gram-Charlier) was applied to S5, but refinement did not lead to better statistical indices; no significant features were modeled, and the Gram-Charlier coefficients values were highly correlated with the S5 positional parameters. Furthermore, at the end of the multipolar refinement, the anharmonic parameters had values less than the e.s.d.'s and therefore the model was rejected. At the end of HO refinement, the rigid-bond test¹⁵ was applied for non-H atoms: the test is excellent with an average value of $\langle \Delta \rangle = 9.4 \times 10^{-4} \text{ \AA}^2$, and the maximum discrepancy being $\Delta = 3.8 \times 10^{-3} \text{ \AA}^2$ for the C9–N10 bond.

B. Multipolar refinement: A radial function study involving sulfur atoms

Refinement strategy. Among the large number of electron density studies (EDS) performed nowadays only few of them have been carried out involving S atoms.^{1,2,16–21} The EDS based on the MOLLY model² use Slater-type radial functions. The MOLLY model describes the atomic electron density as

$$\rho_{\text{at}}(r) = \rho_c(r) + P_\nu \kappa^3 \rho(\kappa r) + \sum_{l=0}^{l_{\text{max}}} \sum_{m=0}^l \kappa'^3 R_{nl}(\kappa' r) P_{lm\pm} y_{lm\pm}(\theta, \varphi),$$

where ρ_c is the spherically symmetric Hartree-Fock core electron density, ρ_v is the spherically averaged free-atom Hartree-Fock valence electron density normalized to one electron, κ and κ' are the expansion-contraction parameters of, respectively, the spherical valence shell and the valence multipoles, $y_{lm\pm}$ are real spherical harmonic angular functions, P_ν and $P_{lm\pm}$ are the population parameters, and $R_{nl}(\kappa' r)$ the Slater-type radial functions defined as

$$R_{nl}(r) = \frac{\alpha^{n+3}}{(n+2)!} r^n e^{-\alpha r}$$

where $n = n_l \geq l$ is required for proper Coulombic behavior satisfying Poisson's equation²² as $r \rightarrow 0$. The α parameter for each atom is set to $\alpha = 2\langle \zeta \rangle$ (since $\rho \propto |\Psi|^2$), where $\langle \zeta \rangle$ is the averaged orbital exponent from the ground states of the valence orbitals wave functions calculated for the Hartree Fock–self consistent field (HF-SCF) free atom.²³ As the total charge for each spherical harmonic function is defined as zero [a value of $P_{lm\pm} = +1$ ($l \neq 0$) means that one electron moves from the negative to the positive lobes in its associated spherical harmonic function $y_{lm\pm}(\theta, \varphi)$], the net atomic charges in the MOLLY model are calculated as

$$q = Z - (N_{\text{core}} + P_\nu + P_{00}),$$

where Z is the number of protons, N_{core} is the number of core electrons and $P_\nu + P_{00}$ is the number of electrons in the valence shell. In this paper, P_{00} is set to zero and the resulting net charge is therefore estimated from the spherical valence density only.

In the multipolar refinement of the title compound no chemical constraints were imposed to any atom; only crystallographic m symmetry was imposed on S5, C1, C7, and C8. The thermal and positional parameters obtained from the HO refinement, and the scale factor from all data refinement (this value only differs from the HO scale factor by 0.2%), were used as starting parameters. Hydrogen atoms were found by difference Fourier syntheses ($\sin \theta/\lambda < 0.5 \text{ \AA}^{-1}$) and refined isotropically. Then, their coordinates were shifted by extending along the $\text{C}_{sp^3}\text{-H}$ and $\text{C}_{sp^2}\text{-H}$ bond vectors to average bond distance values from neutron diffraction (respectively, to 1.085 and 1.076 \AA).²⁴ These distances were kept fixed during all further refinements. The core and radial valence scattering factors $\langle j_0 \rangle$ for the nonhydrogen atoms were calculated from Clementi wave functions,²⁵ and a bound atom form factor for hydrogen²⁶ was used by imposing a starting κ value of 1.16 to the scattering factor of the free hydrogen atom. The real and imaginary dispersion corrections to the form factors given by Cromer²⁷ were used in the structure factor calculations. The Becker-Coppens extinction model²⁸ was initially applied, but values were found to be insignificant; then no extinction model was finally included in the refinement.

The multipolar refinement strategy [$0 < \sin \theta/\lambda < 1.35 \text{ \AA}^{-1}$, $N_{\text{obs}} = 5145$, $I > 3\sigma(I)$] was performed with the following steps: (a) scale factor, (b) P_ν then κ , (c) P_ν and κ ,

TABLE I. Test of the sulfur radial function parameters $[n_l; \alpha(\text{bohr}^{-1})]$; α_f represents the final exponential radial function parameter. Least-squares statistical factors are defined as: $R(F) = \Sigma \Delta / \Sigma F_{\text{obs}}$, $R_w(F) = (\chi^2 / \Sigma w F_{\text{obs}}^2)^{1/2}$, and $S = [\chi^2 / (N_{\text{obs}} - N_{\text{par}})]^{1/2}$, where $\chi^2 = \Sigma w \Delta^2$, $\Delta = (k^{-1} F_{\text{obs}}) - F_{\text{calc}}$, $w = 1/\sigma^2(F_{\text{obs}})$, and N_{obs} and N_{par} are, respectively, the number of data and the number of refined parameters.

	$n = n_l$				α	$\alpha_f = \alpha \kappa'$		$0 < \sin \theta / \lambda < 1.35 \text{ \AA}^{-1}$, $N_{\text{obs}} = 5145$, $I > 3\sigma(I)$				
	$l=1$	$l=2$	$l=3$	$l=4$		S2	S5	$R(F)$	$R_w(F)$	S	$\Sigma w \Delta^2$	k^{-1}
Set A	4	4	4	4	3.60	4.06(2)	4.02(4)	0.0225	0.0219	0.910	4250	0.295 90(9)
					3.85	4.20(2)	4.27(5)	0.0225	0.0219	0.910	4246	0.295 90(9)
					3.95	4.24(2)	4.36(5)	0.0225	0.0219	0.910	4245	0.295 90(9)
					4.10	4.32(2)	4.52(5)	0.0225	0.0219	0.910	4245	0.295 90(9)
Set B	4	4	6	6	3.60	4.49(2)	4.47(4)	0.0225	0.0220	0.914	4282	0.295 92(9)
					3.85	4.60(2)	4.66(4)	0.0225	0.0220	0.913	4273	0.295 92(9)
					3.95	4.67(2)	4.75(4)	0.0225	0.0220	0.912	4270	0.295 91(9)
					4.10	4.78(2)	4.87(4)	0.0225	0.0220	0.912	4265	0.295 91(9)
Set C	6	6	4	4	3.60	4.38(3)	3.76(4)	0.0226	0.0220	0.913	4282	0.295 92(9)
					3.85	4.54(3)	3.96(4)	0.0225	0.0220	0.912	4272	0.295 92(9)
					3.95	4.60(2)	4.04(4)	0.0225	0.0220	0.912	4269	0.295 92(9)
					4.10	4.68(2)	4.18(4)	0.0225	0.0220	0.912	4265	0.295 92(9)
Set D	6	6	6	6	3.60	4.78(2)	4.17(3)	0.0226	0.0221	0.916	4306	0.295 92(9)
					3.85	4.97(2)	4.40(4)	0.0225	0.0220	0.914	4289	0.295 91(9)
					3.95	5.04(2)	4.49(4)	0.0225	0.0220	0.914	4283	0.295 91(9)
					4.10	5.11(2)	4.64(4)	0.0225	0.0220	0.913	4275	0.295 91(9)

(d) P_{lm} , (e) P_v , κ , and P_{lm} , (f) κ' , (g) positional, and U_{ij} parameters for non-H atoms, P_v , κ , and P_{lm} , (h) κ' , (i) all refined parameters together (except κ') and (j) κ' . At each step, the refinement was cycled until convergence. After each heavy atom xyz refinement, the H atoms coordinates were shifted according to average distances observed from neutron experiments²⁴ and hydrogen isotropic thermal motion was adjusted ($\sin \theta / \lambda < 0.5 \text{ \AA}^{-1}$). The deformation terms were extended to dipolar (H atoms), octopolar (N and C atoms) and hexadecapolar (S atoms) levels; the $(n_l; \alpha)$ parameters used for H, C, and N atoms were (1; 2.26 bohr⁻¹), (2, 2, 3; 3.0 bohr⁻¹), and (2, 2, 3; 3.8 bohr⁻¹), respectively.

Optimization of the sulfur radial function. We have recently shown that the Slater radial function of second row atoms must be optimized;^{29,30} thus, for sulfur we have tested several reasonable combinations of $(n_l; \alpha)$ radial function parameters (see sets A, B, C, and D in Table I), including the free atom value²³ [$\alpha = 2\langle \zeta \rangle = (2\zeta_{3s} + 4\zeta_{3p})/3 = 3.85 \text{ bohr}^{-1}$] and the molecule-optimized value³¹ ($\alpha = 4.10 \text{ bohr}^{-1}$), by performing multipolar refinements. For each initial set of $(n_l; \alpha)$ values, Table I shows the statistical indices at the convergence and the refined exponential parameter calculated as $\alpha_f = \alpha \kappa'$. The R factors are almost equivalent from set to set and only inspection of the minimized function $\Sigma w \Delta^2$ [see Fig. 2(a)] may permit us to find some slight differences at convergence: (a) for each set of the n_l parameters, $\Sigma w \Delta^2$ decreases systematically when α increases from 3.60 to 4.10 bohr⁻¹, (b) this behavior is almost linear, and (c) the absolute value of the slope increases with the value of n_l . No statistically significant differences are found between final scale factors (see Table I) and they only differ from the HO scale factor by 0.8%. Thus, all convergences are achieved with excellent internal consistency; this is also supported by the very similar results of the rigid-

bond tests (see later). Furthermore, whatever the initial choice of α , within reasonable limits, the refined α_f values increase for both S2 and S5 atoms. This behavior is also linear as a function of the starting α parameters [see Figs. 2(b) and 2(c)]. We also point out that, comparing α_f e.s.d.'s and rigid-bond test results, the internal S2 atoms are more accurately parametrized than the external S5 atoms.

The residual electron density defined as

$$\Delta \rho_{\text{res}}(\mathbf{r}) = \frac{1}{V} \sum_{\mathbf{H}} [k^{-1} F_{\text{obs}}(\mathbf{H}) - F_{\text{mul}}(\mathbf{H})] e^{i\varphi_{\text{mul}}} e^{-2\pi i \mathbf{H} \cdot \mathbf{r}},$$

has been calculated for all sets of $(n_l; \alpha)$ parameters in the C1-S2-C3 and C4-S5-C4 planes. For a given set of n values (set A, see Table I), the difference maps $\Delta(\Delta \rho_{\text{res}}(\mathbf{r})) = \Delta \rho_{\text{setA}, 4.10}(\mathbf{r}) - \Delta \rho_{\text{setA}, \alpha}(\mathbf{r})$ with $\alpha = 3.60$, 3.85, and 3.95 bohr⁻¹, show maximum differences of 0.02, 0.01, and less than 0.01 $e \text{ \AA}^{-3}$, respectively, at the same positions and close to sulfur atoms. In order to discriminate between other n and α values we also have calculated $\Delta(\Delta \rho_{\text{res}}(\mathbf{r})) = \Delta \rho_{\text{setA}, 4.10}(\mathbf{r}) - \Delta \rho_{\text{setX}, \alpha}(\mathbf{r})$, using $X = B, C$, and D with $\alpha = 3.60$, 3.85, 3.95, and 4.10 bohr⁻¹. The maximum differences are close to sulfur atoms, ranging: (a) 0.05–0.07 $e \text{ \AA}^{-3}$ for set B, (b) 0.08–0.11 $e \text{ \AA}^{-3}$ for set C, and (c) 0.06–0.08 $e \text{ \AA}^{-3}$ for set D. These differences decrease when α increases from 3.60 to 4.10 bohr⁻¹. The external estimates of the average error in maps defined as³²

$$\langle \sigma_{\text{ext}}^2 \rangle^{1/2} = \frac{2}{V} \left[\sum_{\mathbf{H}} [k^{-1} F_{\text{obs}}(\mathbf{H}) - F_{\text{mul}}(\mathbf{H})] \right]^{1/2}$$

remain constant for all refinements at $\langle \sigma_{\text{ex}} \rangle = 0.10 e \text{ \AA}^{-3}$, compared to 0.06 $e \text{ \AA}^{-3}$ of the internal estimate³²

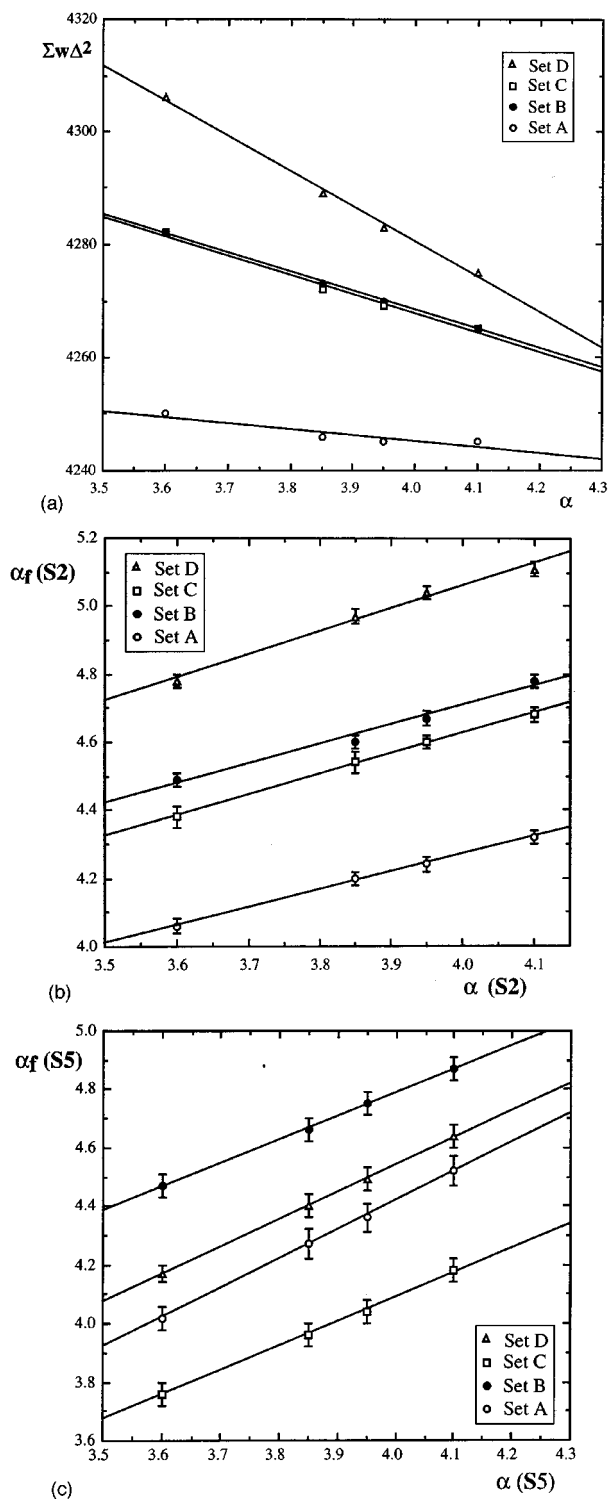


FIG. 2. Estimation of the α parameters of the sulfur radial function: (a) $\Sigma w \Delta^2$ versus α , (b) $\alpha_f(S2)$ versus $\alpha(S2)$, and (c) $\alpha_f(S5)$ versus $\alpha(S5)$. The three graphs are linear regressions and all α and α_f values are in bohr^{-1} units.

$$\langle \sigma_{\text{int}}^2 \rangle^{1/2} = \frac{2}{V} \left[\sum_{\mathbf{H}} [\sigma^2(F_{\text{obs}}(\mathbf{H}))] \right]^{1/2}.$$

The rigid-bond test applied for non-H atoms at convergence show very similar results for all refinements. In all

cases the average value $\langle \Delta_{X,\alpha} \rangle$ is $(7.85 \pm 0.05) \times 10^{-4} \text{ \AA}^2$ and the maximum Δ value involving sulfur atoms is $2.1 \times 10^{-4} \text{ \AA}^2$ for the S5-C4 bond (refinement with set D and $\alpha = 3.85, 3.95$ or 4.10 bohr^{-1}). We therefore conclude that deconvolution between thermal and electron density parameters is excellent for all the chosen sulfur radial functions.

Then, because (a) $\Delta(\Delta\rho_{\text{res}}(\mathbf{r}))$ differences are not statistically significant in relation to the external estimate of the average error in maps, (b) inspection of the $\Delta\rho_{\text{res}}(\mathbf{r})$ maps did not show any improvement compared to set A (see supplementary material), (c) rigid-bond test results are excellent and equivalent for all refinements, and (d) $\Sigma w \Delta^2$ values are systematically minimum in each set when $\alpha = 4.10 \text{ bohr}^{-1}$, we decide to use $n_l = 4, 4, 4$ and $\alpha = 4.10 \text{ bohr}^{-1}$ as starting values of the sulfur radial function in all further calculations. In conclusion, this analysis shows also the limit and the weakness of the multipolar modeling to discriminate between most physically meaningful radial functions.

Positional and thermal parameters from this refinement are listed in Table II. Bond distances and angles and intermolecular short contacts, as well as the list of the F_0/F_c data, are given in supplementary material.⁴⁵

IV. RESULTS AND DISCUSSION

A. Molecular charge-density delocalization

Figure 3 shows the residual electron density in the C1-S2-C3 and C4-S5-C4 planes and in the (010) plane, which is perpendicular to the BTDMTTF and TCNQ molecules. The Fourier summation included 3385 observed structure factors with $\sin \theta/\lambda < 1.0 \text{ \AA}^{-1}$ and $I > 3\sigma(I)$. In spite of very good data and good convergence of the least-squares refinement, an unusually high residual density is found close to the tilted rings and in the lone pair region of S5.³³ This has to be related to the very noticeable residual peaks appearing between stacks of molecules [Fig. 3(c)], probably due to the delocalization of the electron density in the intermolecular region because of the great electron interaction between stacks. This also shows one of the weaknesses of the refinement: it does not fit well the intermolecular residuals due to the limited extension of the radial functions around atomic positions and also due to the difficulty modeling electron density features not directly assigned to specific atoms. Because the $\langle \sigma_{\text{int}}^2 \rangle^{1/2}$ value is significantly lower than these residuals, we investigated whether these features (which are more important than the noise level) could be related to some bad measurements. After convergence of multipolar refinement, we rejected reflections with $|F_{\text{obs}} - F_{\text{mul}}| > 2$ [28 only from the 5145 used in the refinement with $1.7 < |F_{\text{obs}} - F_{\text{mul}}|/\sigma(F_{\text{obs}}) < 6.5$; these 28 reflections were found everywhere in the reciprocal space) and we recalculated the Fourier differences in the same planes; we found similar residuals which magnitudes are reduced by less than $0.05 e \text{ \AA}^{-3}$. In order to know the contribution of a delocalized electron density distribution between molecules to the structure factors, we considered a bath of an equidistributed (and overestimated) $\rho = 0.2 e \text{ \AA}^{-3}$ between BTDMTTF molecules in the unit cell: the maximum effect obtained on the 28 rejected reflections was 1.1% for (020) and the other reflections were affected by less than 0.5%. This effect has a

TABLE II. Fractional coordinates, anisotropic thermal parameters for non-H and isotropic thermal parameters for H atoms (with e.s.d.'s) from refinement A ($\alpha = 4.10 \text{ bohr}^{-1}$). The form of the temperature factor used is $T = \exp(-2\pi^2 \sum_i \sum_j h_i h_j a^{*i} a^{*j} U^{ij})$.

Atom	x	y	z	U^{11}	U^{22}	U^{33}	U^{12}	U^{13}	U^{23}
S2	0.930 87(0)	-0.118 03(1)	0.155 42(3)	0.008 23(3)	0.007 92(2)	0.015 28(4)	0.000 49(2)	0.002 77(2)	0.000 11(3)
S5	0.758 85(1)	0	0.576 84(4)	0.008 96(4)	0.011 01(4)	0.011 75(5)	0	0.003 62(3)	0
N10	0.699 84(2)	-0.178 42(3)	-0.049 79(12)	0.020 41(14)	0.011 00(11)	0.028 00(18)	0.003 88(10)	0.007 62(13)	-0.002 86(12)
C1	0.970 68(2)	0	0.067 43(14)	0.007 47(13)	0.008 90(14)	0.014 56(18)	0	0.002 62(12)	0
C3	0.864 35(2)	-0.053 79(3)	0.297 00(9)	0.008 20(9)	0.008 49(9)	0.012 66(12)	0.000 05(7)	0.002 26(8)	0.000 02(9)
C4	0.806 56(2)	-0.108 34(3)	0.413 14(10)	0.009 88(10)	0.009 34(10)	0.014 25(13)	-0.000 60(8)	0.003 23(9)	0.000 42(9)
C6	0.526 83(2)	-0.098 25(3)	0.410 82(10)	0.010 09(10)	0.007 88(9)	0.014 08(13)	0.000 22(8)	0.003 59(9)	-0.000 19(9)
C7	0.556 00(2)	0	0.314 41(13)	0.008 73(13)	0.008 04(13)	0.011 90(17)	0	0.002 29(12)	0
C8	0.610 57(2)	0	0.126 78(14)	0.009 23(14)	0.008 30(13)	0.013 38(18)	0	0.003 12(13)	0
C9	0.639 10(2)	-0.097 02(3)	0.029 96(10)	0.011 60(11)	0.009 18(10)	0.016 01(14)	0.000 86(8)	0.004 10(10)	-0.000 79(10)
H41	0.733 47(-)	-0.150 44(-)	0.195 30(-)	0.010 9(24)					
H42	0.816 03(-)	-0.166 36(-)	0.618 28(-)	0.010 1(28)					
H6	0.548 71(-)	-0.172 19(-)	0.342 28(-)	0.014 0(25)					

magnitude approximately equal to the difference found between the multipolar and the observed structure factor (1.5%) for the (020) reflection. Then this highly delocalized charge density in the intermolecular BTDMTTF regions induces small effects on the structure factors, making very difficult both its experimental measurement and its modeling through a multipolar refinement.

On the other hand, these residual peaks could be related with the CDW modulation. This instability around the average positions, observed by the x-ray diffuse scattering experiment, is usually quite small, making atomic displacements typically about 1% of the interatomic spacing.³⁴ However, as both $4k_F$ and $2k_F$ instabilities are very small at $T = 130 \text{ K}$ (they completely disappear at $T = 80 \text{ K}$),⁷ they do not affect significantly the crystal structure at $T = 130 \text{ K}$ and therefore the structure factors. In that way, CDW should not be responsible for the unusually high residual peaks found between molecules, which could be related to the high electron interaction because of the very short intermolecular distances along stacks. We then note that these very small instabilities at this temperature permit the electron density study of BTDMTTF-TCNQ.

B. Deformation electron density around sulfur atoms

Figures 4 and 5 show the experimental dynamic electron density deformation defined as³⁵

$$\Delta\rho_{\text{exp}}(\mathbf{r}) = \frac{1}{V} \sum_{\mathbf{H}} (k^{-1} F_{\text{obs}}(\mathbf{H}) e^{i\varphi_{\text{mul}}} - F_{\text{sph}}(\mathbf{H}) e^{i\varphi_{\text{sph}}}) e^{-2\pi i \mathbf{H} \cdot \mathbf{r}},$$

around sulfur atoms and in the TCNQ plane, respectively. The $\Delta\rho_{\text{exp}}(\mathbf{r})$ maps give an estimation of the quality of measurements and include the effects of both finite experimental resolution and convolution with the atomic thermal parameters. In our case, they also reflect the strong electron density interaction effect between molecules. Experimental deformation maps were calculated from set A with α

$= 4.10 \text{ bohr}^{-1}$; the Fourier summation included 3385 observed structure factors with $\sin \theta/\lambda < 1.0 \text{ \AA}^{-1}$ and $I > 3\sigma(I)$.

Figure 4(a) gives the deformation electron density around the S2 atom in the plane bisecting the C1-S2-C3 angle. The internal S2 atom develops an extended lone pair in the sp^2 hybrid orbital direction, which peaks $0.55 e \text{ \AA}^{-3}$ at 0.3 \AA from S2 centered on the bisecting line. Figure 4(b), which is a view perpendicular to both Fig. 4(a) and the cation plane, shows that the S2 π -electron system is polarized in the S2 . . . S2 direction (i.e., along the c axis, see Fig. 1). Figure 4(c) (C4-S5-C4' bisecting plane) shows that the external sulfur S5 develops the electron density of its lone pair in three peaks, one occupying a trigonal planar sp^2 hybrid orbital and the other two belonging to a perpendicular $p\pi$ orbital. Figure 4(d) [deformation electron density in the same plane as Fig. 3(c)] reveals that one of the two π peaks is polarized towards the C8-C9 \equiv N10 part of the anion belonging to the next closest sheet, pointing out that S5 polarization results from two S5 . . . TCNQ intermolecular effects: the interaction along the [100] direction and the electron interaction that exists with the anion of the closest neighboring sheet.

C. Relations between the structure and the electron density

As previously described,⁶ cations and anions are segregately stacked along the c axis (see Fig. 1), in such a way that each donor column is surrounded by four acceptor columns (and *vice versa*) and that molecules in stacks exhibit the commonly observed “ring-over-bond” overlap arrangement.

As shown in Fig. 5 (see also short contact distances in supplementary material), crystal packing between cation and anion stacks is governed by intermolecular interactions originated from N10 and C9. Figure 5 shows the very important interaction existing between the external S5 sulfur atom and the triple bond electron density $C\equiv N$: the minimal distance between S5 and the TCNQ anion does not concern C9 but the triple bond [the angle formed by S5, the middle point between C9 and N10, and N10 (C9) is 92.5° (87.5°)]. This

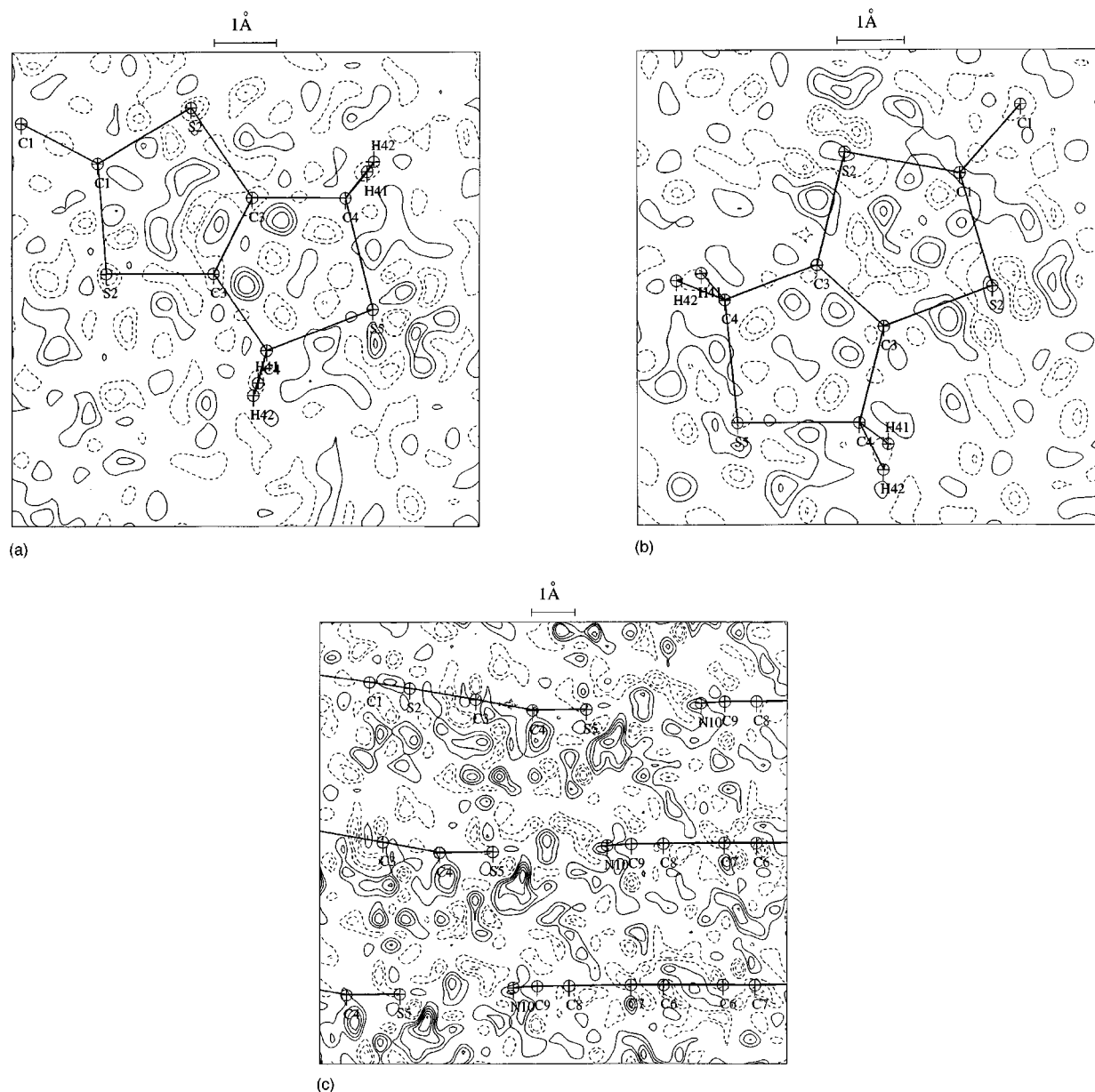


FIG. 3. Residual electron density from set A refinement ($\alpha=4.10 \text{ bohr}^{-1}$) in the planes: (a) C1-S2-C3, (b) C4-S5-C4', and (c) (010), this latter plane being perpendicular to BTDMTTF and TCNQ ions. In all of them, the label of the atoms which are out of plane are also projected onto the planes. Contours intervals are at $0.05 e \text{ \AA}^{-3}$ level; solid lines are positive, dotted lines are negative, and the zero contour is omitted.

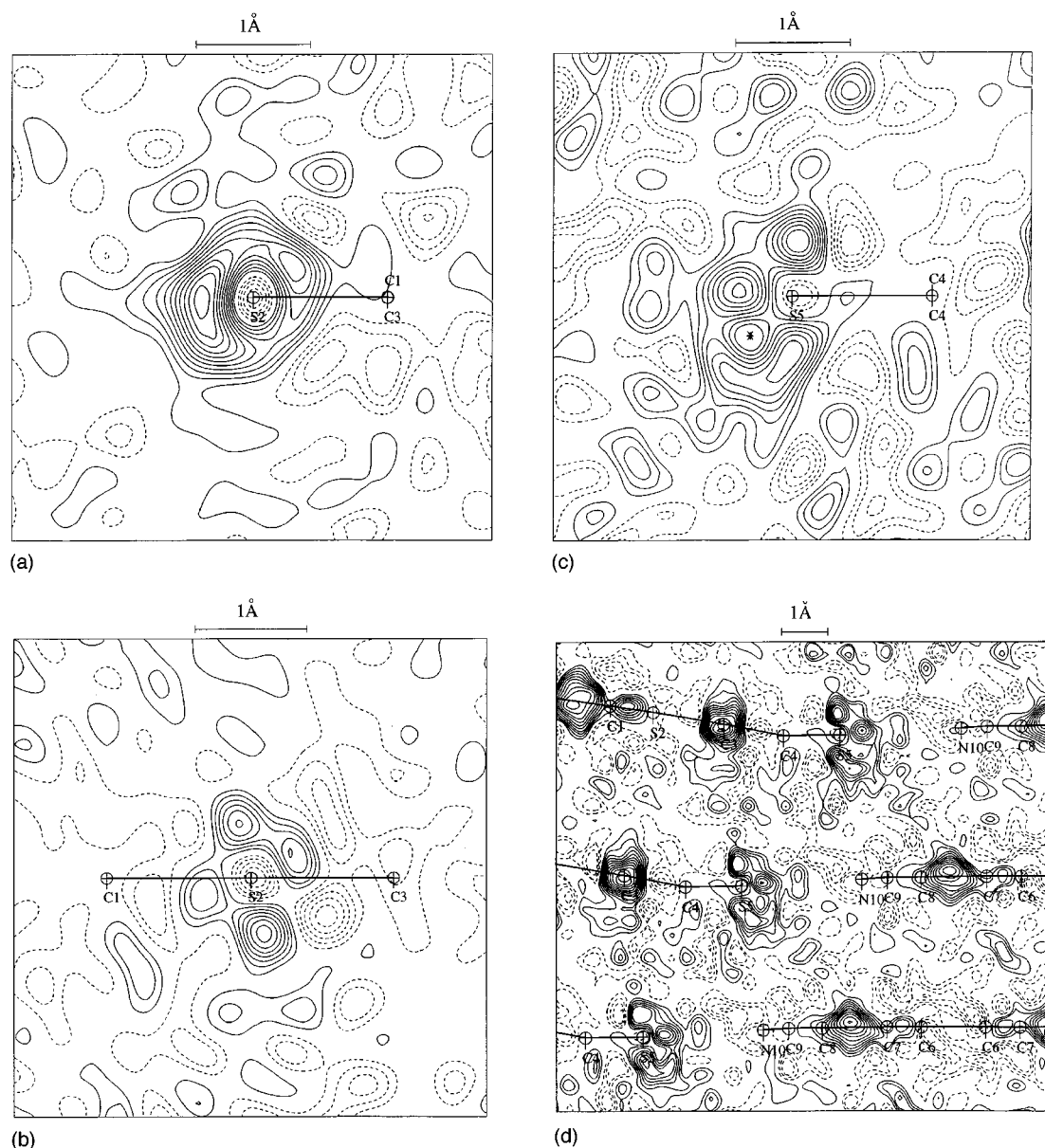
S5... (C \equiv N) interaction induces several structural effects: (a) S5 goes into the cavity limited by TCNQ arms, leading to an angle of 0.6° between the TCNQ and C4-S5-C4' planes, (b) nitrogens surround S5 from both sides, making TCNQ arms as pincers [$d_{S5\dots N10}=3.4394 \text{ \AA}$, $\alpha((C8-C9-N10)=177.0^\circ$, $\tau_{C7-C8-C9-N10}=26.2^\circ$], and (c) the strong interaction between S5 and the C9-N10 TCNQ arms explains that the C4-S5-C4 plane is tilted 9.2° from the rest of the cation plane towards the TCNQ anion. When temperature decreases from RT to $T=130 \text{ K}$ this tilt angle increase to 10.2° : as the angle between the *c* axis and the perpendicular direction to TCNQ anions (34.4°) is greater than that formed by BTDMTTF cations (24.2°), the decrease of temperature reduces more distances between anions than cations ($d_{\text{BTDMTTF}}=3.541$ and 3.521 \AA , $d_{\text{TCNQ}}=3.256$ and 3.184 \AA , $c=3.928$

and 3.859 \AA , respectively, for RT and $T=130 \text{ K}$) and the resulting effect is the observed increase of this tilt angle. The shortening of the TCNQ... TCNQ distance by cooling is in relation to the decrease of resistivity⁶ and can explain that conductivity is mainly due to the electrons moving along *c* through TCNQ anions.⁷

TCNQ presents a *deviation* from the formal quinoid pattern defined by the alternation of C-C single and double bonds. All these distances have intermediate values between single and double bonds (see supplementary material). As shown in Fig. 4, the maximum of the deformation electron density at the formal C6-C7 and C8-C9 single bonds [0.55 and $0.60 e \text{ \AA}^{-3}$, respectively, for $d_{C6-C7}=1.4363(4) \text{ \AA}$ and $d_{C8-C9}=1.4176(4) \text{ \AA}$] are higher than that of the formal C7-C8 double bond [$0.45 e \text{ \AA}^{-3}$ for $d_{C7-C8}=1.3998(7) \text{ \AA}$].

TABLE III. Statistics of fit ($R_1 = \Sigma|\Delta|/\Sigma U_{\text{obs}}$ and $R_2 = (\Sigma\Delta^2/\Sigma U_{\text{obs}}^2)^{1/2}$, where $\Delta = U_{\text{obs}} - U_{\text{calc}}$), principal mean-square amplitudes (librational L_{ij} and translational T_{ij}) and torsion angles $\langle\varphi^2\rangle$ of the group C9-N10 around both axes [010] and the perpendicular to TCNQ anion passing through C8 atom. Results are given for independent cation and anion entities at both temperatures (RT and $T = 130$ K).

		$\times 10^5$ (rad ²)				$\times 10^4$ (Å ²)				b axis $\langle\varphi_1^2\rangle$ (deg ²)	perp TCNQ $\langle\varphi_2^2\rangle$ (deg ²)	R_1	R_2
		L_{11}	L_{22}	L_{33}	L_{13}	T_{11}	T_{22}	T_{33}	T_{13}				
BTDMTTF	RT	255 (74)	2 (1)	0 (2)	10 (6)	230 (9)	251 (85)	303 (49)	43 (9)			8.3	8.0
	130 K	82 (21)	1 (0)	0 (1)	4 (2)	83 (3)	98 (24)	85 (14)	24 (3)			6.7	6.4
TCNQ	RT	468 (204)	25 (9)	13 (11)	31 (18)	290 (25)	41 (203)	0 (144)	80 (26)			18.0	19.4
	130 K	215 (56)	7 (4)	9 (4)	7 (5)	114 (10)	0 (69)	17 (62)	38 (11)			16.1	19.9
TCNQ	RT	0 (2)	0 (1)	0 (1)	0 (1)	250 (11)	234 (18)	335 (22)	24 (12)	77.5 (9.5)	5.7 (2.6)	8.5	8.7
	130 K	0 (1)	0 (0)	0 (0)	0 (0)	95 (4)	82 (7)	125 (8)	22 (5)	36.9 (3.7)	2.8 (1.0)	7.7	8.4



This effect is compensated by the more cylindrical shape of the C7-C8 bonding electron density, which involves a greater volume of electron density deformation. All these features agree with an extended electronic resonance along the molecule and with the topology of the electron density in this molecule, which shows similar Laplacian and total electron density at the critical points in those bonds (see Sec. IV F).

If we compare the almost linear C—C≡N group with that found in tetrafluoroterephthalonitrile³⁶ (TFP) at $T=98$ K, the C-C distance is shorter and C≡N is longer in our material [$d_{\text{C}\equiv\text{N}}=1.1593$ (5) versus 1.149 Å and $d_{\text{C-C}}=1.4176$ (4) versus 1.433 Å]. This is probably due to both charge transfer toward N10 (see Sec. IV D) and to the many intermolecular interactions involving this atom. The C8-C9 bond peak (see Fig. 5) is $\approx 0.2 e \text{ Å}^{-3}$ higher than that corresponding in TFP, in relation with its shorter distance. However, in our study, the C≡N bond peak is also $0.2 e \text{ Å}^{-3}$ higher in spite of a longer bond length. Furthermore the TCNQ nitrogen lone pair is also $0.25 e \text{ Å}^{-3}$ higher than that observed in TFP. As supported by Secs. IV D and IV F, these effects can be interpreted in terms of cation charge transfer, mainly absorbed by nitrogens. This charge transfer induces a repulsive Coulombic force between C9 and N10 atoms, that compensate the covalent effect of a higher C≡N electron density bond peak, and makes the observed distances C≡N longer and C—C shorter in BTDMTTF-TCNQ.

The rigid-bond test shows that the highest differences involve C8—C9 and C9—N10 bonds (1.3×10^{-3} and $3.9 \times 10^{-3} \text{ Å}^2$, respectively): their movements are more influenced by the translational and the librational vibrations of the anion because these atoms are placed at the external positions of the TCNQ arms. Table III shows the results of the TLS (translation, libration, screw) correction³⁷ calculated with the hypothesis that the cation and the anion are two independent rigid bodies. The C9-N10 group was considered either as an attached rigid group rotating around the [010] axis and around an axis perpendicular to TCNQ (both passing through C8), or not. Inspection of Table III shows that

whereas the cation librates only around [100] direction, the libration of the anion is found to be different if the C9-N10 group is allowed to rotate around the two axes or not. The thermal parameters fit is much better when rotations are allowed. In conclusion, the hypothesis of two independent rigid bodies seems to end at realistic results if translational and librational motions of the anion are described allowing the rotations of the C9-N10 group.

D. Charge transfer and dipole moment

Atomic net charges and charge transfer between BTDMTTF and TCNQ molecules were calculated from the multipolar refinement described previously, which gives a charge migration from the BTDMTTF cation to the TCNQ anion (see refinement I in Table IV). We also performed another multipolar refinement imposing that BTDMTTF transfers charge only from the external sulfurs S5 to the TCNQ anions (see refinement II in Table IV). Refinements I and II were performed imposing electroneutrality constraint (i.e., the total charge in the unit cell was set to zero) at each cycle of refinement. Both refinements led to the same statistical indices and to statistically equivalent atomic charges, confirming the hypothesis of refinement II: charge is transferred from S5 atoms ($\approx 0.34e$ for each S5, i.e., $\approx 0.7e$ from the cation) to TCNQ ($\approx -0.7e$). In the anion, the transferred charge is absorbed by the C9≡N10 groups (each group bears $\approx -0.2e$, i.e., $\approx -0.8e$ for all C≡N groups in the anion), mainly concentrated on the nitrogen atoms (see discussion in Sec. IV F) and for a small part on both the C9 atoms and the triple bonds (in relation with the high electron density bond peak of the C≡N bond, as pointed out in Sec. IV C).

In the previous paper,⁷ x-ray diffuse scattering and tight-binding calculations agree with an electron transfer from BTDMTTF to TNCQ increasing when cooling; the diffuse scattering measurements and the IR and Raman frequency measurements at RT suggest a charge transfer of $\rho_{\text{RT}} \approx 0.5e$. Furthermore, the relative variation of $\Delta\rho/\rho$ when cooling from 295 to 130 K is $\approx 12.5\%$, corresponding to an estimated total charge transfer of $\rho_{130\text{ K}} \approx 0.56e$. If we assume that all the electron transfer comes from S5, this means that S5 must have a net atomic charge of $+0.28e$, in close agreement with our result [$q_{\text{S5}} = +0.34(3)e$].

As initially shown,⁷ whereas BTDMTTF-TCNQ exhibits relevant $4k_F$ x-ray diffusion lines at RT (which disappear on cooling about 80 K), it does not exhibit a well-defined $2k_F$ CDW instability (which becomes critical at low temperature). As the electronic properties of BTDMTTF-TCNQ strongly resemble those of TTF-TCNQ (which has a well-defined $2k_F$ CDW), there is no apparent reason for nonexistence of $2k_F$ instability. In fact, the x-ray diffuse scattering experiment at 100 K shows that this instability really occurs but with a very weak scattering vector. If we suppose that the atomic net charge of S5 at RT is just $0.25e$ (the charge transfer from the cation to the anion at RT is $0.5e$),⁷ and increase on cooling (as observed from our results), this means that, on average, one over four S5 atoms supply one electron to the TCNQ neighbors. However, if $4k_F$ instabilities are much better defined than $2k_F$ instabilities (on the difference with the TTF-TCNQ complex), this could be due to the fact that

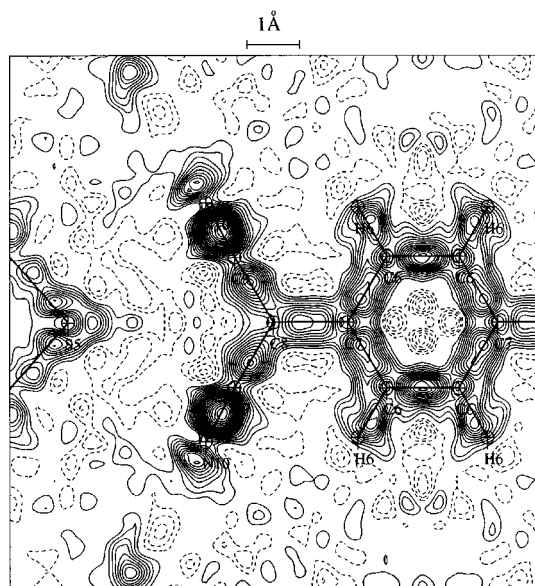


FIG. 5. Experimental electron density deformation in the plane C6-C7-C8 of the anion (labels and contours as in Fig. 3).

TABLE IV. Atomic net charges (in e) in the asymmetric unit, and net charges of the ions from refinement I and refinement II. In the latter, we constrained the charge to be transferred only from S5 to the anion. In both cases, the radial function parameters for sulfur atoms were those from set A with $\alpha=4.10$ bohr $^{-1}$. Atomic net charges are given with three digits in order to show the electroneutrality in the complex.

	C1	S2	C3	C4	H41	H42	S5
Multipolar I	-0.444 (28)	+0.365 (21)	-0.171 (19)	-0.500 (21)	+0.251 (13)	+0.300 (15)	+0.328 (34)
Refinement II	-0.454(26)	+0.356(20)	-0.178(16)	-0.512(20)	+0.259(13)	+0.301(15)	+0.336(30)
	N10	C9	C8	C7	C6	H6	TCNQ
+0.75	-0.139 (19)	-0.075 (23)	-0.074 (30)	+0.088 (31)	-0.045 (19)	+0.065 (17)	-0.75
+0.67	-0.135 (18)	-0.071 (22)	-0.066 (28)	+0.092 (31)	-0.039 (18)	+0.065 (16)	-0.67

one over eight S5 atoms supply two electrons rather than one over four S5 atoms supply one electron. This hypothesis is supported by the voltamperometric studies of the BTDMTTF donor:¹⁰ it is shown that the first and the second ionization potentials are closer (0.55 and 0.72 V) than in TTF (0.39 and 0.62 V); in that way, S5 try to release electrons by pairs. As well as temperature decrease and charge-transfer increase, the $4k_F$ instability becomes less favorable as more than one S5 atoms (of each four contiguous BTDMTTF molecules) may transfer electrons to the TCNQ stacks. The nonequivalence of the S5 atoms explains also the important residual ($0.25e \text{ \AA}^{-3}$) which shows up in this neighborhood [see Fig. 3(c)].

The dipole moment μ of the complex was calculated in the crystal axis system from the multipole parameters of refinement II (as described in a previous work³⁸). The components and the modulus of the dipole moment are $\mu = (33.6, 0, 18.6)$ and $|\mu| = 37(3)$ Debye. As long as the dipole moment measures the anion-cation interaction and as charge transfer mainly involves S5, the angle between μ and the C8-S5 direction (4.8°) is intermediate between those found with the cation (angle between μ and C1'-C1 direction is 174.1°) and with the anion (angle between μ and C8'-C8 direction is 2.5°). As previously pointed out,³⁸ the net charges contribution (≈ 35 Debye) is much greater than the atomic dipoles contribution (≈ 2 Debye). Whereas the large component of the dipole moment in the crystal **a** axis is obviously due to the position of the complex along this direction, the component along the crystal **c** axis is in relation to the relative tilt angle between the cation and the anion stacks with **c** [$\alpha(\mu, \mathbf{c}) = 58.6^\circ$].

E. Electrostatic potential of BTDMTTF-TCNQ complex removed from the crystal lattice

Electrostatic potential calculations around the pseudoisolated molecules were performed using the ELECTROS program³⁹ with the multipolar parameters from refinement II (plots from refinements I and II show very similar features, see supplementary material).⁴⁵ In that way, all information on the molecular groups (obtained from the crystal) was used to calculate the electrostatic potential function for the donor [Fig. 6(a)], the acceptor [Fig. 6(b)] and the complex donor-acceptor [Fig. 6(c)]. As expected, whereas the cation devel-

ops a positive potential everywhere around the molecule, because of the preponderant contributions of sulfur and hydrogen positive atoms, the anion develops a negative potential everywhere around its molecular van der Waals surface, due to the preponderant contribution of the highly negative region N10-C9, which even overcompensates the positive contribution of the internal H6 hydrogens. The first positive contour in Fig. 6(a) ($+0.05e \text{ \AA}^{-1}$) and the $-0.05e \text{ \AA}^{-1}$ outer negative contour in Fig. 6(b) do not appear in the plots because they are placed far away from both donor and acceptor. In both cases, these latter contours have an ellipsoidal shape centered in the molecules. When both molecules are placed at the donor-acceptor geometry positive and negative regions are in competition in the intermolecular region. This produces a saddle point topology in the electrostatic potential. This conformation and the electrostatic potential value at this site ($\approx 0.08e \text{ \AA}^{-1}$, corresponding to an energy of ≈ 1.15 eV for a positive unit point charge) are typical of those found for hydrogen bonds⁴⁰ (HB). Thus, the topological signature of the electrostatic potential in the intermolecular space between molecules involved in charge-transfer properties is a saddle in the region of maximum interaction.⁴¹

F. Topology of the electron density

The electron density of BTDMTTF-TCNQ complex has been modeled and topologically characterized, with particular emphasis on the properties of the intermolecular density distribution. The topological characterization was accomplished using the PROP program written by Souhassou (1992).⁴² According to Bader,⁴³ the real-space points \mathbf{r}_{CP} , where $\nabla\rho(\mathbf{r}_{CP})=0$ (called critical points, CP) and their associated topological properties (as the Hessian matrix eigenvalues $\lambda_1, \lambda_2, \lambda_3$ and eigenvectors, the electron density ρ and the ellipticity ε) characterize both atoms and their interactions. In this way, the CP's positions as well as the Laplacian and the gradient vector field of the electron density were calculated at the crystal geometry for the pseudoisolated BTDMTTF [Figs. 7(a) and 7(b)] and BTDMTTF-TCNQ complex [Figs. 7(c) and 7(d)]. Negative and positive $\nabla^2\rho(\mathbf{r})$ values correspond, respectively, to regions where the electron density is locally concentrated and depleted. Because of the relationship between $\nabla^2\rho(\mathbf{r})$ and the potential and kinetic energies through the local form of the Virial's

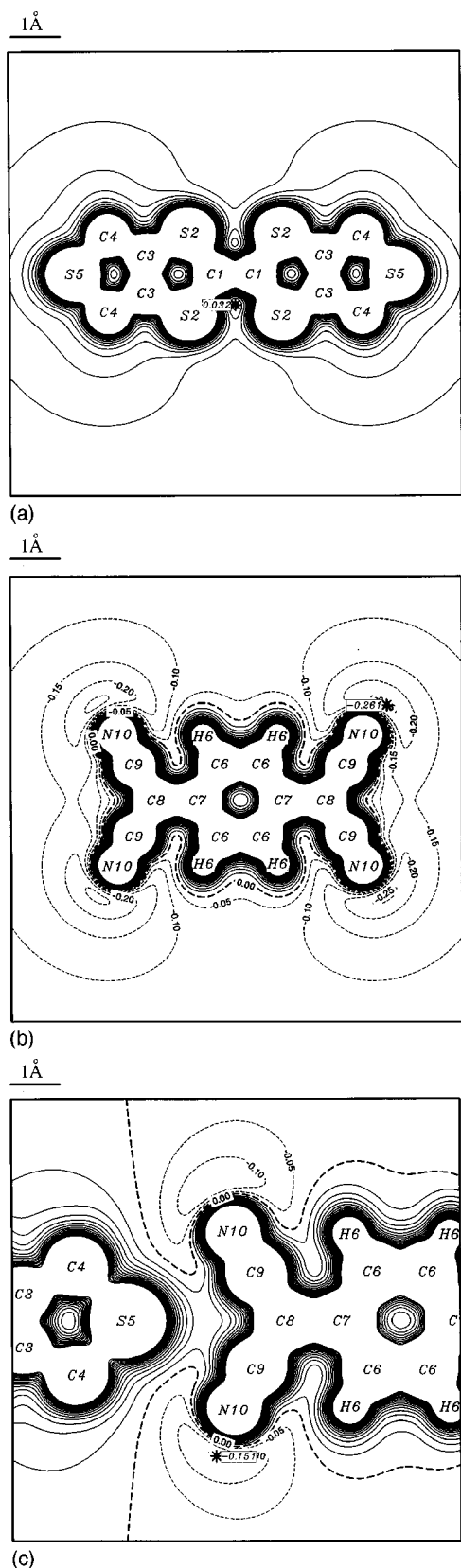


FIG. 6. Electrostatic potential in the planes of the pseudoisolated: (a) cation, (b) anion, and (c) the complex cation-anion. Contours intervals are at $0.05 e \text{ \AA}^{-1}$; solid lines are positive, dotted lines are negative, and the zero contour is a broken line. The minimum value on each plot is marked by *.

theorem,⁴³ $\nabla^2 \rho(\mathbf{r})$ is negative in regions where the potential energy contribution of the electrons is in excess over twice its kinetic energy. Table V shows the topological characterization of the $(3, -1)$ CP's (bonding interactions) and $(3, +1)$ CP's (ring interactions) in the BTDMTTF-TCNQ complex. In the cation, the more negative $\nabla^2 \rho(\mathbf{r})$ values and the highest $\rho(\mathbf{r}_{\text{CP}})$ values are found for the $\text{C1}=\text{C1}'$ and $\text{C3}=\text{C3}'$ $(3, -1)$ CP's, leading to a high concentration of $\rho(\mathbf{r})$ around carbons involved in the double bonds [Fig. 7(a)]. Their ellipticities at the CP's [$\varepsilon(\mathbf{r}_{\text{CP}}) = 0.21$ and 0.28 , respectively] are the highest found in the cation, showing their π character, specially for the $\text{C3}=\text{C3}'$ interaction. On the other hand, the electron density that is concentrated in $\text{S}-\text{C}$ covalent bonds is significantly smaller, and especially for the external S5 (see Table V). The electron density at the S5-C4 critical point is smaller than that observed for the corresponding S2-C bonds ($1.08 e \text{ \AA}^{-3}$ compared to 1.31 and $1.34 e \text{ \AA}^{-3}$, respectively), which is in relation to the longer S5-C4 bond length. We also note that the Laplacian at the S5-C4 critical point is less negative than that observed for S2-C critical points ($-0.52 e \text{ \AA}^{-5}$ compared to -2.39 and $-3.10 e \text{ \AA}^{-5}$, respectively); hence the kinetic energy contribution at the S5-C4 critical point is greater. All these observations show that S5 shares a significantly less electron density with C4 carbon than S2 does with C1 and C3 (which are involved in the highest electron concentration regions of BTDMTTF), and thus, from this point of view, S5 appears more isolated from the rest of the cation. This effect validates the result of tight-binding extended Hückel calculations,⁷ which shows that the external sulfur S5 orbitals do not contribute to the highest occupied molecular orbital, contrary to S2 which is involved by a significant coefficient of -0.40 .

The concentration of electron density in TCNQ is significantly higher than in BTDMTTF [see Figs. 7(a) and 7(c)] which is obviously in relation to their associated anion and cation characters. Whereas in the cation the electron density is mainly concentrated around atoms involved in double bonds, in the anion, $\rho(\mathbf{r})$ is concentrated around all TCNQ bonds, and especially around nitrogens. Looking at the $\nabla^2 \rho(\mathbf{r}_{\text{CP}})$ and $\rho(\mathbf{r}_{\text{CP}})$ values in the TCNQ carbon chain of covalent bonds (Table V), we found a slight increase of covalence from $\text{C9}-\text{C8}$ to $\text{C6}-\text{C6}'$ bonds. The double character of the $\text{C}-\text{C}$ bonds is better described by the bond ellipticity than from the total electron density at the CP: whereas $\text{C6}=\text{C6}'$ has a more prominent double-bond character than $\text{C7}=\text{C8}$, as shown by $\rho(\mathbf{r}_{\text{CP}})$ and $\varepsilon(\mathbf{r}_{\text{CP}})$ values ($2.25 e \text{ \AA}^{-3}$ and 0.23 compared to $2.01 e \text{ \AA}^{-3}$ and 0.17 , respectively), the later has a similar $\rho(\mathbf{r}_{\text{CP}})$ value compared to the other bonds of the carbon chain $\text{C9}-\text{C8}=\text{C7}-\text{C6}$ (1.91 , 2.01 , and $1.98 e \text{ \AA}^{-3}$, respectively) and it can be only distinguished by the $\varepsilon(\mathbf{r}_{\text{CP}})$ value (0.10 , 0.17 , and 0.11 , respectively). Furthermore, the bonding characteristics of $\text{C6}=\text{C6}'$ in TCNQ are very similar to those of $\text{C1}=\text{C1}'$ and $\text{C3}=\text{C3}'$ in BTDMTTF (see Table V). Especially noticeable is the electron density concentration around nitrogens, as can be seen in Fig. 7(c), where the magnitudes of the Laplacian attain values of up to $60 e \text{ \AA}^{-5}$ in the bond and lone pair regions. This effect is in relation to the charge transfer from S5, mainly absorbed by nitrogens, as was pointed out before.

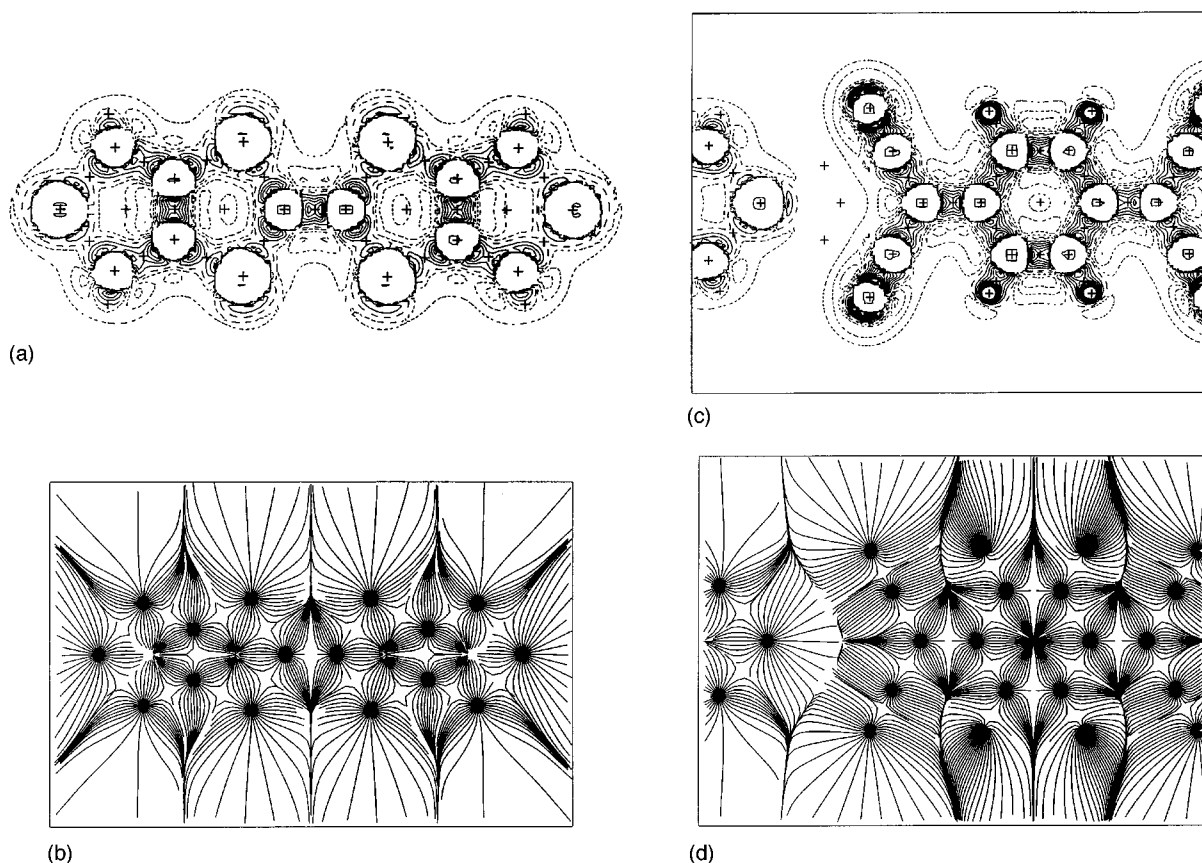


FIG. 7. (a) $\nabla^2\rho(\mathbf{r})$ and (b) $\nabla\rho(\mathbf{r})$ functions of BTDMTTF in the cation plane, (c) $\nabla^2\rho(\mathbf{r})$ and (d) $\nabla\rho(\mathbf{r})$ functions of the complex BTDMTTF-TCNQ in the C9-S5-C9' plane. In the Laplacian maps, the negative contours (solid lines) are at $4 e \text{ \AA}^{-5}$ intervals, the positive contours (dotted lines) are at $2 e \text{ \AA}^{-5}$ intervals, and the zero contour is a broken line. The CP positions are marked by +.

The triple bond $\text{C9}\equiv\text{N10}$ is topologically characterized by the very high magnitudes of both $\rho(\mathbf{r}_{\text{CP}})$ and curvatures. Whereas the high positive curvature leads to a strong depletion of $\rho(\mathbf{r})$ along the bond path to the nuclear attractors, the high magnitudes of the negative curvatures (for the two perpendicular directions to the bond path) compensate for this effect, inducing a very high electron density concentration at the CP. Because the magnitudes of the two curvatures are very similar, the π character along the two associated directions compensates each other in the calculus of $\varepsilon(\mathbf{r}_{\text{CP}})$, resulting in a cylindrical symmetry of the $\text{C}\equiv\text{N}$ bond.

The gradient vector field of $\rho(\mathbf{r})$ for the pseudoisolated cation and for the complex are represented in Figs. 7(b) and 7(d), respectively. These figures show the atomic basins, i.e., the space regions associated with each nuclear attractor of $\rho(\mathbf{r})$ which are defined by the (3,-3)-type CP's. The trajectories associated with the (3,-1) CP's define the interatomic surfaces, which are shared by adjacent atoms. The bond path, which is the interaction path between two local maxima of $\rho(\mathbf{r})$ and not necessarily being the shortest one, cuts perpendicularly the interatomic surface through the (3,-1) CP. The gradient vector field found around S5 in the pseudoisolated cation, is modified in presence of the anion due to the intermolecular interaction. In fact, Fig. 7(d) clearly shows that the S5 intermolecular interaction is not made with N10 (even if charge transfer is mainly absorbed by these atoms) neither with C9 (even if S5-C9 is the smallest interatomic distance between the two considered ions) but with

the triple bond⁴⁴ $\text{C9}\equiv\text{N10}$. This interaction explains the existence of the $\text{S5}\dots(\text{C9}\equiv\text{N10})$ (3,-1) CP, which is revealed by the $\nabla^2\rho(\mathbf{r})$ map⁴⁴ [see Fig. 7(c)]. In this way, the (3,-1) CP associated with the triple bond behaves as a two-dimensional attractor, which is a very exceptional case. To our knowledge this is the first experimental observation of such a critical point. As interactions involving two-dimensional attractors are unstable, the bond path will flip from the (3,-1) triple bond CP to the (3,-3) CP of C9 or N10, and *vice versa*, with a very small change in energy, because the electron density in the $\text{S5}\dots\text{TCNQ}$ intermolecular region is very flat. In that way, even if the bond path flips to the three-dimensional attractors the $\text{S5}\dots$ triple bond interaction will remain predominant. The low value of $\rho(\mathbf{r}_{\text{CP}})$ is a reflection of the ionic character of both fragments of the complex. Because of the creation of two (3,-1) CP's between S5 and triple bonds placed at both TCNQ arms, there is necessarily a (3,+1) CP. This latter CP appears as a ring interaction, in the same way as for the internal rings in BTDMTTF and TCNQ, which are created by closed bond paths going through the local maxima of $\rho(\mathbf{r})$. Thus, at (3,+1) CP's, $\rho(\mathbf{r})$ is locally depleted because of the surrounding attractors.

In summary, the minimal distance between the external sulfur atom and the TCNQ anion is not with C9 but with the triple bond CP, interacting with each other in order to transfer the electronic charge from S5 to the anion and, through triple bonds, as far as nitrogens, where it is highly concen-

TABLE V. Topological characterization of the (3,−1) and the (3,+1) critical points (CP) in the BTDMTTF-TCNQ complex. The $\lambda_1, \lambda_2, \lambda_3$ ($e \text{ \AA}^{-5}$) are the curvatures of the three principal axes of the Hessian matrix, $\nabla^2\rho = \lambda_1 + \lambda_2 + \lambda_3$ ($e \text{ \AA}^{-5}$) is the Laplacian of the electron density, ρ ($e \text{ \AA}^{-3}$) is the electron density and ϵ is the ellipticity value [only defined for (3,−1) CP], at the CP. The values d_A and d_B (\AA) represent the distances from the (3,−1) CP to the attractors *A* and *B*.

CP	<i>A</i> – <i>B</i>	d_A	d_B	$\lambda_1, \lambda_2, \lambda_3$	$\nabla^2\rho$	ρ	ϵ
(3,−1)	C1–C1′	0.688	0.688	12.75, −13.62, −16.45	−17.32	2.16	0.21
(3,−1)	C1–S2	0.838	0.909	12.99, −7.32, −8.06	−2.39	1.34	0.10
(3,−1)	S2–C3	0.916	0.823	12.80, −7.35, −8.55	−3.10	1.31	0.16
(3,−1)	C3–C3′	0.674	0.674	13.38, −14.47, −18.47	−19.56	2.32	0.28
(3,−1)	C3–C4	0.772	0.723	11.93, −10.54, −11.01	−9.63	1.67	0.04
(3,−1)	C4–S5	0.866	0.962	11.21, −5.61, −6.12	−0.52	1.08	0.09
(3,−1)	C6–C6′	0.682	0.682	13.13, −14.83, −18.22	−19.91	2.25	0.23
(3,−1)	C6–C7	0.721	0.715	13.48, −13.29, −14.79	−14.60	1.98	0.11
(3,−1)	C7–C8	0.675	0.725	13.65, −12.90, −15.11	−14.36	2.01	0.17
(3,−1)	C8–C9	0.686	0.731	14.77, −12.55, −13.85	−11.64	1.91	0.10
(3,−1)	C9–N10	0.475	0.685	31.69, −29.88, −31.25	−29.44	3.58	0.05
(3,−1)	S5–Triple bond	1.759	≈1.606	0.65, −0.06, −0.10	0.49	0.04	0.61

CP	Involved ring	$\lambda_1, \lambda_2, \lambda_3$	$\nabla^2\rho$	ρ
(3,+1)	Internal ring of BTDMTTF	2.48, 1.75, −0.66	3.58	0.24
(3,+1)	External ring of BTDMTTF	2.38, 2.32, −0.95	3.75	0.28
(3,+1)	Internal ring of TCNQ	1.91, 1.66, −0.31	3.26	0.13
(3,+1)	Intermolecular ring S5-TCNQ	0.34, 0.10, −0.06	0.37	0.03

trated. The C9≡N10 CP, acting as a two-dimensional attractor, leads charge transfer from the donor to the acceptor through the S5... (C9≡N10) CP, which behaves as a bridge. That mechanism implicitly controls the electronic properties that depend on charge transfer as, for instance, conductivity and CDW phenomena. On the other hand, the charge transfer interaction between the external sulfur atom and the triple bond is topologically similar to a weak HB, which is characterized by a (3,−1) CP with a low value of $\rho(\mathbf{r}_{\text{CP}})$ and a small positive magnitude of $\nabla^2\rho(\mathbf{r}_{\text{CP}})$.

Finally, the analysis developed in this paper seems to demonstrate the important role of the S5 atom in the electronic properties of BTDMTTF-TCNQ. The strong intermolecular S5 contacts introduce a stiffening in the donor-acceptor chains. They are probably the origin of the blocking of CDW instabilities at low temperature, retaining the metallic state until about 26 K. However, to draw a definitive conclusion we will perform a similar study in a related ma-

terial of the TTF-TCNQ family, having similar properties but without an external sulfur atom.

ACKNOWLEDGMENTS

This work has been supported by the PB93-0119 grant from Dirección General de Investigación Científica y Técnica (DGICYT), the University Henri Poincaré, the CNRS (URA 809) and the CNI/MAT community (Calcul Numérique Intensif en Sciences des Matériaux). E. Espinosa thanks the Ministerio de Educación y Ciencia for financial support. We are grateful to Dr. N. E. Ghermani and Dr. M. Souhassou for help in the calculations of electrostatic potential and the topology of the electron density and to Dr. C. Rovira and Dr. J. Veciana for kindly supplying the BTDMTTF-TCNQ high-quality crystals. We are also very grateful to Professor R. F. W. Bader for helpful discussions in the topological analysis of the electron density.

* Author to whom correspondence should be addressed.

¹P. Coppens, T. N. Guru Row, P. Leung, E. D. Stevens, P. J. Becker, and Y. W. Yang, *Acta Crystallogr. Sec. A* **35**, 63 (1979).

²N. K. Hansen and P. Coppens, *Acta Crystallogr. Sec. A* **34**, 909 (1978).

³R. F. Stewart, *J. Chem. Phys.* **58**, 1668 (1973); R. F. Stewart and M. A. Spackman, *VALRAY: Users Manual*, Chemistry Department, Carnegie-Mellon University, Pittsburgh, PA, 1983.

⁴B. M. Craven, H. P. Weber, and X. He, *The POP Procedure: Computer Programs to Derive Electrostatic Properties from Bragg Reflections*, University of Pittsburgh, Pittsburgh, 1987.

⁵F. L. Hirshfeld, *Acta Crystallogr. Sec. B* **27**, 769 (1971); F. L.

Hirshfeld, *Isr. J. Chem.* **16**, 226 (1977).

⁶N. Santaló, J. Tarrés, E. Espinosa, J. Llorca, E. Molins, J. Veciana, C. Rovira, M. Mays, S. Yang, D. O. Cowan, C. Garrigou-Lagrange, J. Amiel, P. Delhaes, and E. Canadell, *Synth. Met.* **55–57**, 2050 (1993).

⁷C. Rovira, J. Tarrés, J. Llorca, E. Molins, J. Veciana, S. Yang, D. O. Cowan, C. Garrigou-Lagrange, J. Amiel, P. Delhaes, E. Canadell and J. P. Pouget, *Phys. Rev. B* **52**, 8747 (1995).

⁸C. K. Johnson, *Computer program to plot thermal ellipsoids*, 1968, ORNL Lab, USA.

⁹N. Santaló, J. Veciana, and C. Rovira, *Tetrahedron Lett.* **30**, 7249 (1989).

¹⁰C. Rovira, J. Veciana, N. Santaló, J. Tarrés, J. Cirujeda, E. Mo-

- lins, J. Llorca, and E. Espinosa, *J. Org. Chem.* **59**, 3307 (1994).
- ¹¹R. J. Nelmes, Z. Tun, and W. F. Kuhs, *Ferroelectrics* **71**, 125 (1987). In fact, the temperature of transition was found between 121.7 and 123 K, depending on the deuteration level of the sample.
- ¹²R. H. Blessing, *Crystallogr. Rev.* **1**, 3 (1987).
- ¹³R. H. Blessing, *J. Appl. Crystallogr.* **22**, 396 (1989).
- ¹⁴G. De Titta, *J. Appl. Crystallogr.* **18**, 75 (1985).
- ¹⁵F. L. Hirshfeld, *Acta Crystallogr. Sec. A* **32**, 239 (1976).
- ¹⁶C. Cohen-Addad, M. S. Lehmann, P. Becker, and H. Davy, *Acta Crystallogr. Sec. B* **44**, 522 (1988).
- ¹⁷Y. Wang, M. J. Chen, and C. H. Wu, *Acta Crystallogr. Sec. B* **44**, 179 (1988).
- ¹⁸B. Fabius, C. Cohen-Addad, F. K. Larsen, M. S. Lehmann, and P. Becker, *J. Am. Chem. Soc.* **111**, 5728 (1989).
- ¹⁹J. Buschmann, T. Koritsanszky, R. Kuschel, P. Luger, and K. Seppelt, *J. Am. Chem. Soc.* **113**, 233 (1991).
- ²⁰Y. Wang, S. K. Yeh, S. Y. Wu, C. T. Pai, C. R. Lee, and K. J. Lin, *Acta Crystallogr. Sec. B* **47**, 298 (1991).
- ²¹B. N. Figgis, B. B. Iversen, F. K. Larsen, and P. A. Reynolds, *Acta Crystallogr. Sec. B* **49**, 794 (1993).
- ²²R. F. Stewart, *Isr. J. Chem.* **16**, 124 (1977).
- ²³E. Clementi and D. L. Raimondi, *J. Chem. Phys.* **38**, 2686 (1963).
- ²⁴F. Allen, *Acta Crystallogr. Sec. B* **42**, 512 (1986).
- ²⁵E. Clementi, *IBM J. Res. Dev. (Suppl.)* **9**, 2 (1965).
- ²⁶R. F. Stewart, E. R. Davidson, and W. T. Simpson, *J. Chem. Phys.* **43**, 175 (1965).
- ²⁷D. T. Cromer, *International Tables for X-Ray Crystallography*, edited by J. A. Ibers and W. E. Hamilton (Kynoch, Birmingham, England 1974), p. 148.
- ²⁸P. J. Becker and P. Coppens, *Acta Crystallogr. Sec. A* **30**, 129 (1974).
- ²⁹E. Espinosa, Ph.D. thesis, University of Barcelona, Spain, 1994.
- ³⁰G. R. Moss, M. Souhassou, R. H. Blessing, E. Espinosa, and C. Lecomte, *Acta Crystallogr. Sec. B* **51**, 650 (1995).
- ³¹W. J. Hehre, R. Ditchfield, R. F. Stewart, and J. A. Pople, *J. Chem. Phys.* **52**, 2769 (1970).
- ³²D. W. J. Cruickshank, *Acta Crystallogr.* **2**, 65 (1949).
- ³³Slightly different residual densities appearing between Figs. 3(a) and 3(b) are in relation to the tilt angle between both planes [$\approx 10.2(4)^\circ$]; whereas C4 lies at 0.03 Å from the C1-S2-C3 plane, the external sulfur atom S5 lies at -0.19 Å.
- ³⁴R. E. Thorne, *Phys. Today* **49(5)**, 42 (1996).
- ³⁵P. Coppens, in *Electron Distributions and the Chemical Bond*, edited by P. Coppens and M. B. Hall (Plenum, New York, 1982), pp. 61–92.
- ³⁶P. Seiler, W. B. Schweizer, and J. D. Dunitz, *Acta Crystallogr. Sec. B* **40**, 319 (1984).
- ³⁷R. E. Rosenfeld, Jr., N. K. Trueblood, and J. D. Dunitz, *Acta Crystallogr. Sec. A* **34**, 828 (1978); J. D. Dunitz, V. Shomaker, and N. K. Trueblood, *J. Phys. Chem.* **92**, 856 (1988); J. D. Dunitz, E. F. Marevik, and N. K. Trueblood, *Angew. Chem. Int. Ed. Engl.* **27**, 880 (1988).
- ³⁸E. Espinosa, C. Lecomte, E. Molins, S. Veintemillas, A. Cousson, and W. Paulus, *Acta Crystallogr. Sec. B* **52**, 519 (1996).
- ³⁹N. Ghermani, N. Bouhmaida, and C. Lecomte, *ELECTROS*: Computer program to calculate electrostatic properties from high-resolution x-ray diffraction, University of Nancy 1, France, 1992.
- ⁴⁰E. Espinosa, C. Lecomte, N. E. Ghermani, J. Dévemy, M. M. Rohmer, M. Bénard, and E. Molins, *J. Am. Chem. Soc.* **118**, 2501 (1996).
- ⁴¹In some special cases the *saddle* region is the *chair* region because of the surrounding interactions, E. Espinosa, Ph.D. thesis, University of Barcelona, Spain, 1994.
- ⁴²M. Souhassou; *PROP*: Computer program to calculate the experimental multipolar electron density from high-resolution x-ray diffraction. Hauptman Woodward Institute, Buffalo, New York, and University of Nancy 1, France (1992).
- ⁴³R. F. W. Bader, *Atoms and Molecules: a Quantum Theory*, International Series of Monographs on Chemistry, edited by J. Halpen and M. L. H. Green (Clarendon, Oxford, 1990).
- ⁴⁴In spite of the low $\rho(\mathbf{r}_{\text{CP}})$ value, this feature (the former reported to our knowledge) is supported by two facts: (a) the existence of the (3, −1) CP is evidenced by the great magnitude of the positive curvature in relation to the smaller negatives ones, and (b) the positive curvature is placed along the direction between S5 and the triple bond region.
- ⁴⁵See AIP Document No. PAPS-B15-PRBMDO-56-1820 for 54 pages of (Tables—supplementary material). Order by PAPS number and journal reference, from American Institute of Physics, Physics Auxiliary Publication Service, Carolyn Gehlbach, 500 Sunnyside Boulevard, Woodbury, New York 11797-2999. Fax: 516-576-2223, e-mail: paps@aip.org. The price is \$1.50 for each microfiche (98 pages) or \$5.00 for photocopies of up to 30 pages, and \$0.15 for each additional page over 30 pages. Air-mail additional. Make checks payable to the American Institute of Physics in U.S. dollars drawn on a U.S. bank.